

Minimally invasive implantable fetal micropacemaker: mechanical testing and technical refinements

Li Zhou¹ · Adriana Nicholson Vest¹ · Raymond A. Peck¹ · Jonathan P. Sredl¹ · Xuechen Huang¹ · Yaniv Bar-Cohen^{2,3} · Michael J. Silka^{2,3} · Jay D. Pruetz^{2,3,4} · Ramen H. Chmait⁴ · Gerald E. Loeb¹

Received: 28 May 2015 / Accepted: 15 February 2016
© International Federation for Medical and Biological Engineering 2016

Abstract This paper discusses the technical and safety requirements for cardiac pacing of a human fetus with heart failure and hydrops fetalis secondary to complete heart block. Engineering strategies to meet specific technical requirements were integrated into a systematic design and implementation consisting of a novel fetal micropacemaker, a percutaneous implantation system, and a sterile package that enables device storage and recharging maintenance in a clinical setting. We further analyzed observed problems on myocardial fixation and pacing lead fatigue previously reported in earlier preclinical trials. This paper describes the technical refinements of the implantable fetal micropacemaker to overcome these challenges. The mechanical performance has been extensively tested to verify the improvement of reliability and safety margins of the implantation system.

Keywords Pacemaker · Epicardial · Fetal · Heart block · Hydrops fetalis

✉ Li Zhou
zhou15@usc.edu

¹ Medical Device Development Facility, Department of Biomedical Engineering, Viterbi School of Engineering, University of Southern California, 1042 Downey Way, Los Angeles, CA 90089, USA

² Division of Cardiology, Department of Pediatrics, Children's Hospital of Los Angeles, 4650 Sunset, Los Angeles, CA 90027, USA

³ Keck School of Medicine, University of Southern California, 1975 Zonal Ave, Los Angeles, CA 90033, USA

⁴ Division of Maternal-Fetal Medicine, Department of Obstetrics and Gynecology, Keck School of Medicine, University of Southern California, 1300 North Vermont Avenue, Suite 710, Los Angeles, CA 90027, USA

1 Introduction

Complete atrioventricular block (CAVB), also known as third-degree heart block, in a human fetus is a rare condition associated with significant mortality if comorbidity is present [5, 17, 27, 32]. Fetal bradycardia due to complete heart block can progress in utero to hydrops fetalis, which usually results in fetal demise or neonatal death due to extreme prematurity or multi-organ system failure [13, 21]. For isolated CAVB without structural heart defects, the fetal cardiac conduction pathway is believed to be damaged by the transplacental passage of maternal autoimmune antibodies [1, 19, 39]. Pharmacologic and immunologic therapies have been attempted to reverse or halt the progression of the CAVB, but the benefits are minimal [14, 15, 17, 34, 36, 38]. For adult patients, the presence of CAVB is an accepted indication for cardiac pacemaker placement to ensure an adequate heart rate [29]. Similarly, successfully pacing a hydropic fetus with CAVB during the fetal period should theoretically resolve the heart failure and edema in 3–4 weeks and may permit an otherwise normal gestation. A conventional epicardial pacemaker could then be placed after delivery as required to sustain a physiological heart rate [12].

1.1 State-of-the-art

Over the past three decades, fetal pacing has been attempted by several investigators, but no survivor of fetal pacing has been reported [2, 6, 40]. All the experiences indicate that the fetal heart can be paced electrically but that the mechanical constraints including lead anchorage, deployment, and attachment in utero require a novel strategy.

1.2 Safety and technical requirements

Minimally invasiveness

- The entire pacing system should be delivered through a cannula or catheter in order to avoid open surgery (hysterotomy), which poses unacceptable risks to mother and the pregnancy [3, 8, 16].
- Accurate placement will require real-time imaging using ultrasound or fetoscopy [23]. Fetuses with hydrops develop fluid collections in the pleural and pericardial spaces, so ultrasonic visualization and access to those spaces are achievable.

Myocardial fixation

- The electrode should penetrate into the myocardium from the epicardial surface and stably anchor in the ventricular wall and deliver electrical current to surrounding myocytes.
- The insertion process should result in minimal trauma to the myocardium.

Adaptation to fetal anatomy

- The entire pacemaker system must be within the fetus to avoid dislodgement and other lead complications from fetal movement.
- The motion between the electrode and the electronics package with each heartbeat and chest movement must be accommodated by a flexible lead that is strong enough to withstand the strain yet flexible enough to minimize stress on the myocardial fixation site in order to minimize inflammation, fibrosis, and loss of healthy myocytes at the electrode–tissue interface [7].
- The required lead fatigue life is about 3 million cycles (3 months at 100 bpm), which is substantially lower than a conventional pacing lead.

Electronic requirements

- CAVB is a rare condition, estimated at around 500 cases/year in the USA [26], so development and manufacturing costs need to be kept low.
- The fetus with CAVB demands steady and continuous ventricular pacing for the remainder of the gestation following device implant, and the fetal pacemaker is meant to be replaced by conventional pacemaker after birth [11, 29].
- The fetal pacemaker must function for up to 3 months depending on the gestational age of the fetus. Given the small size mandated above, the power cell will have to be recharged at least once in utero [26].

- The charge status of the battery must be monitored both in utero and in the sterile package while awaiting implantation.

The aims of this paper are to present our technical development of a fetal pacemaker implantation system that meets all the above requirements, describe the device fabrication techniques, report the experimental data from the animal studies, and summarize the mechanical tests performed to validate the design changes.

2 Methods

2.1 Micropacemaker and implantation system

A design concept for a fetal pacemaker has been presented previously [26]. The fully fabricated and functional device prototype in its implantation system is illustrated in Fig. 1.

The fetal pacemaker functions in a fixed-rate mode (i.e., VOO) with a rate that predictably varies with the battery voltage (in the range of 100–110 bpm). The 3-mAh cell can sustain a typical stimulus output pulse of 3 μC (3 V peak, 250 μs time constant) for 6 days [26]. The pacing circuit design permits inductive recharging via a large (40 cm diameter) external primary coil that can be placed over the mother's abdomen, as described elsewhere [26]. Both the state of charge and the rate of recharging of the lithium cell can be inferred from small changes in the output rate of the pacemaker. After implantation, the brief but relatively intense stimulus pulses in the fetus generate widespread stimulus artifact signals that are easily recorded via skin ECG electrodes on the mother's abdomen. During the storage, the pacemaker in its sterile package is connected to a load and its output pulse rate monitored without direct electrical connection.

2.2 Device fabrication

Electronic Assembly Figure 2 illustrates the fabrication sequences of the electronic subassembly.

Pacing Lead The electrode material is pure iridium (Ir) because it can be activated to provide a low-impedance interface with tissue [31, 35]. Both the Ir electrode and the flexible PtIr lead were formed using a bobbin winder (model 1201 plus automatic traverse 1250, Adams-Maxwell, Los Angeles, CA). The tip of the Ir electrode was honed with fine grinding disk (coated abrasive: silicon carbide; 180 grit) mount on a rotary tool. These parameters were subsequently modified in light of experimental

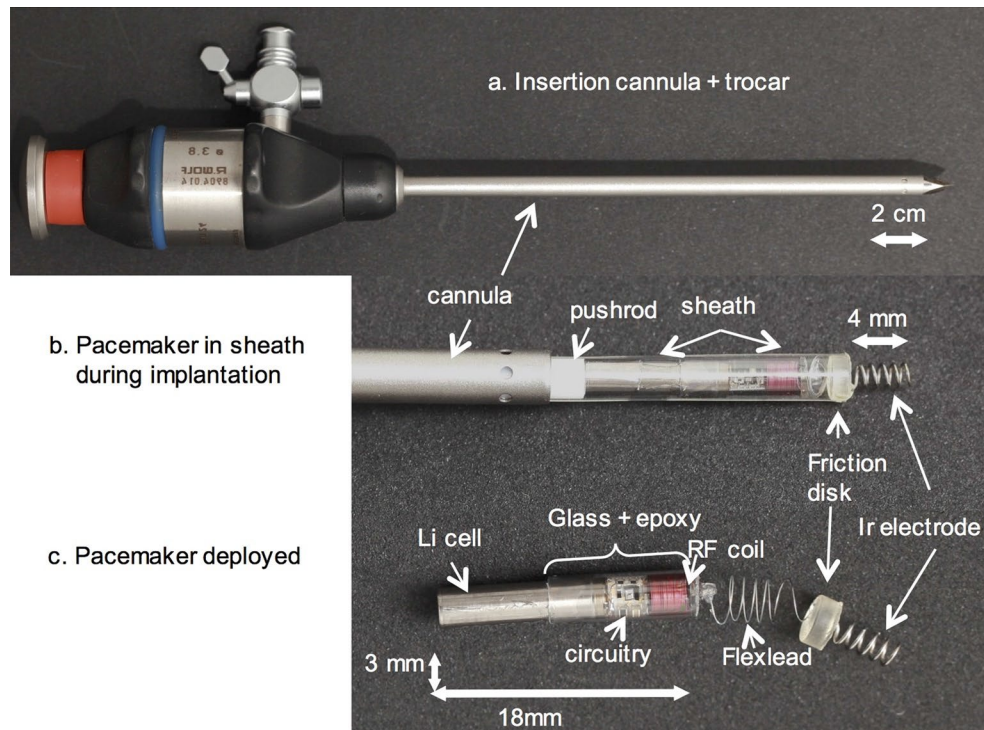


Fig. 1 Fetal micropacemaker and its implantation system. **a** Implantation cannula (4.5 mm o.d. \times 3.8 mm i.d.) with sharpened tip of the trocar protruding from the tip. **b** Configuration during implantation with the micropacemaker inside a polyimide plastic sheath that slides through the cannula. The friction disk is wedged into the end of the sheath, allowing the protruding Ir electrode to be turned into the myocardium (predeployment). The pacemaker is deployed from the sheath by a pushrod after confirming ventricular capture by ultra-

sound. **c** The fetal pacemaker as deployed. Features from *left to right*: battery case of lithium cell, which functions as return electrode; glass sleeve for epoxy encapsulation; printed circuit board with discrete surface-mount circuitry and RF coil for inductive recharging; flexible lead (75 μ m Pt-30Ir with Parylene-C insulation; epoxy friction disk over welded joint, corkscrew electrode (254 μ m Ir with Parylene-C insulation) (this figure is adapted from Bar-Cohen et al. [4])

results (see below). Platinum–iridium alloy was selected for the flexible lead so that it could be resistively welded to both the iridium electrode and the platinum output pin that extends out from the pulse generator epoxy packaging. The lead assembly is insulated with a thin layer of Parylene-C coating (thickness \approx 10 microns). The lead characteristics have been reported in our previous rabbit studies [26]. The resistive weld between the flexible lead and the pure Pt output pin was insulated and mechanically protected with a coating of silicone elastomer (Dow-Corning MED A) for strain relief.

During manufacture and testing of previous versions of the fetal micropacemaker, it was observed that the gripping force of the plastic sheath on the smooth, cylindrical epoxy friction disk was variable and tended to decrease after sterilization in ethylene oxide. A new version with small teeth was fabricated by transfer molding (see below and Fig. 6). The toothed shape was laser-cut into stainless steel (California Lasers Inc.) and embedded in silicone elastomer to provide a negative mold into which the epoxy was poured and cured.

2.3 Functional sterile package design

A functional sterile package holds the fetal micropacemaker during the low-temperature sterilization process with ethylene oxide (EtO), which is commonly selected for medical devices that contain heat-sensitive electronic components such as the Li-ion cell. Figure 3 illustrates the design of the carrier that will be sealed into a Tyvek sterile pouch.

The micropacemaker preloaded in the plastic sheath is contained within a channel on a rigid polycarbonate (PC-ISO) substrate, which is compatible with EtO sterilization. The polymeric substrate is fabricated with plastic jet 3D printing to create slot and groove features with high depth–width ratio. Connection to the Ir electrode (pacing cathode) is provided by a concave copper disk pushed against the electrode tip by a delicate compression spring mechanism (shown in Fig. 3). The copper disk is gold-plated and then coated with a thick layer of electrically conductive silicone elastomer (silver-filled adhesive SS-26 from Silicone Solutions Inc.) to prevent damaging the sharp electrode tip. A spring clip made from phosphor bronze connects to the titanium case of the Li-ion cell (reference electrode) through the

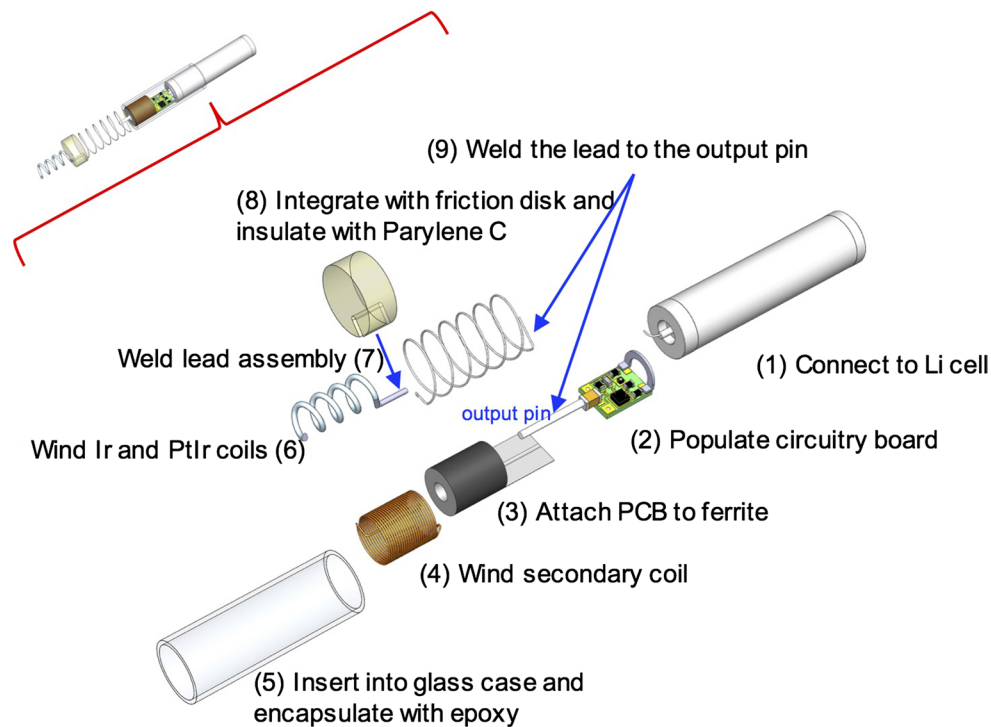


Fig. 2 Exploded view of the fetal pacemaker assembly and sequential manufacturing steps: (1) Weld a nickel wire to the positive terminal of Li-ion cell. (2) Populate the discrete surface-mount electronic components and output pin on ceramic circuit substrate. (3) Mount the circuit on the ledge of the ferrite with the epoxy (302-3 M) and attach the ferrite to the Li-ion cell with the ethyl cyanoacrylate. The nickel-plated titanium horseshoe bracket is soldered to the substrate and laser-welded to the battery titanium case to provide the electrical ground connection as well as the mechanical reinforcement on the

ferrite assembly. (4) Wind the secondary inductive coil on the ferrite using a coil winder. Strip off the insulation near the PCB terminals and solder the wires on the electrical substrate. Electrically activate the device by soldering the nickel wire to the circuit. (5) Clean and insert the electronic assembly into the glass capillary for epoxy encapsulation. (6) Wind iridium coil and PtIr coil. (7) Resistively weld the coil assembly. (8) Integrate with the epoxy friction disk and insulated with Parylene-C. (9) Weld flexible lead to the output pin to complete the micropacemaker

fenestrations on both sides of the plastic sheath. The contact areas with the Li cell case are electroplated with gold coating to avoid oxidation by the EtO sterilant. The two electrodes are wired to a 1-K Ω load in parallel with a light-emitting diode. Once connected, the LED flashes to indicate the output rate of the pacemaker. The carrier with the pacemaker installed is sealed into a pouch with a clear window. The external apparatus (not shown in figure) includes a photodetecting diode to detect the output pulses. The sterile pouch with the pacemaker inside fits into a 5-cm-diameter coil in a benchtop version of the RF recharging system. This design has been iteratively tested and refined with the full cycle of the EtO sterilization to validate the material compatibility and the reliability of the electromechanical linkage system.

2.4 Experimentation

2.4.1 Animal test

The animal study protocol was approved by the Institutional Animal Care and Use Committee at the University

of Southern California and the Los Angeles Biomedical Research Institute. Fetal pacemaker were percutaneously implanted into seven near-term fetal sheep (gestation age at 112–129 days) according to the procedure described by Bar-Cohen et al. [4]. The histology and biocompatibility results can also be found there. The purpose of this paper is to evaluate the mechanical performance of the implants before and after refinements of the design and materials.

The flexible lead is not designed to accommodate the large respiratory movements of adult animals. Testing in a fetal animal model provides a more realistic validation of the open-coiled lead performance. Necropsies were performed before the fetal sheep was delivered, so no breath was taken. We removed a relatively large tissue block surrounding the implants and fixed them by immersion in formalin without excessive handling. We obtained high-resolution X-ray images (Fig. 7) of the tissue block to examine the mechanical integrity of the implanted pacing leads.

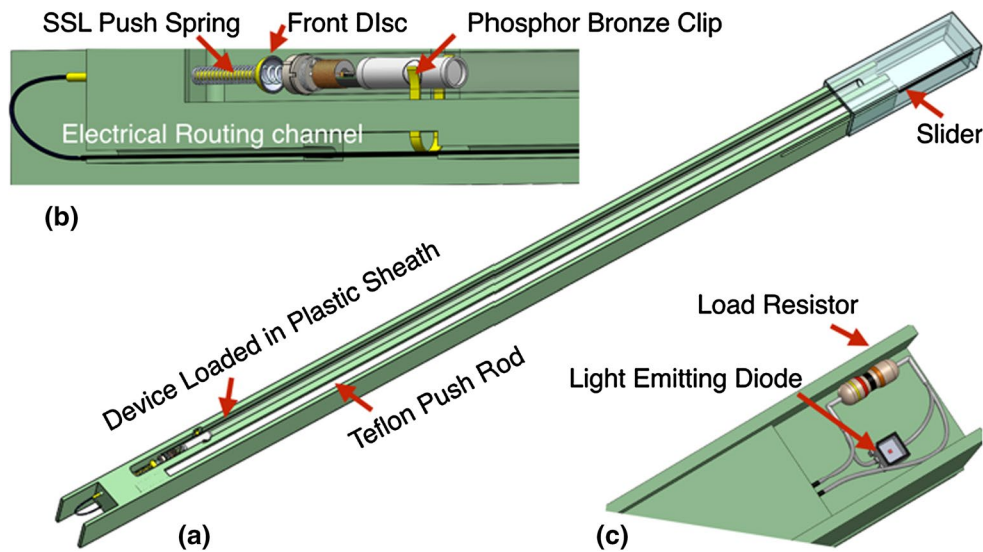


Fig. 3 The design of the functional sterile packaging: The pacemaker loaded in the plastic sheath and the Teflon push rod are carried in individual channels on the substrate (a); the slider retains the proximal ends until ready for use. The electromechanical contact system is detailed in (b). To establish a reliable electrical connection, a delicate compression spring (125 μm stainless steel wire) pushes a concave

copper disk against the Ir electrode tip. The gold-plated phosphor bronze clip clamps on the Li cell case through the fenestration in the plastic sheath. c The micropacemaker is connected to a load resistor in parallel with a light-emitting diode to indicate the pulsing rate, from which the battery charge status can be inferred

2.4.2 Mechanical test on the insertion and release force and torque

Two types of friction disk designs (shown in Fig. 6) were attached to sharpened Ir electrodes and loaded into plastic sheaths. The proximal ends of the sheaths were mounted to a Nano 17 Force/Torque sensor (ATI Industrial Automation; resolution: 1/16 N mm torque and 1/80 N force). The analog signals from the transducer were digitized by a National Instruments DAQ. The rotational torque and axial force required to screw the electrode into a cadaver pig heart and to expel the friction disk from the plastic sheath were recorded and analyzed using a MATLAB program on a personal computer.

3 Results

3.1 Factors affecting electrode penetration

In the first two fetal sheep experiments, the Ir electrode encountered high resistance and was unable to penetrate the myocardium on a total of four attempts [4]. This led us to review our previous acute rabbit experiments [26]. The in vivo implantation results are mapped in Fig. 4. Implantations of Ir electrodes (1.3 mm coil diameter) were generally successful on the left ventricle (LV) but generally less successful on the right ventricle (RV) (see Discussion). The electrode tip tended to snag connective tissues on the RV

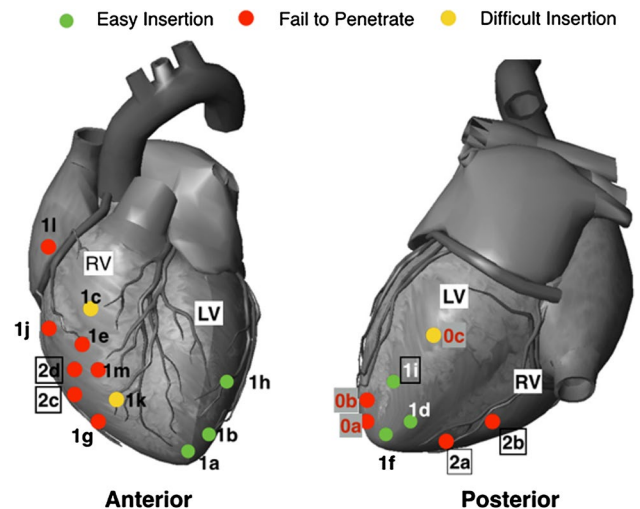
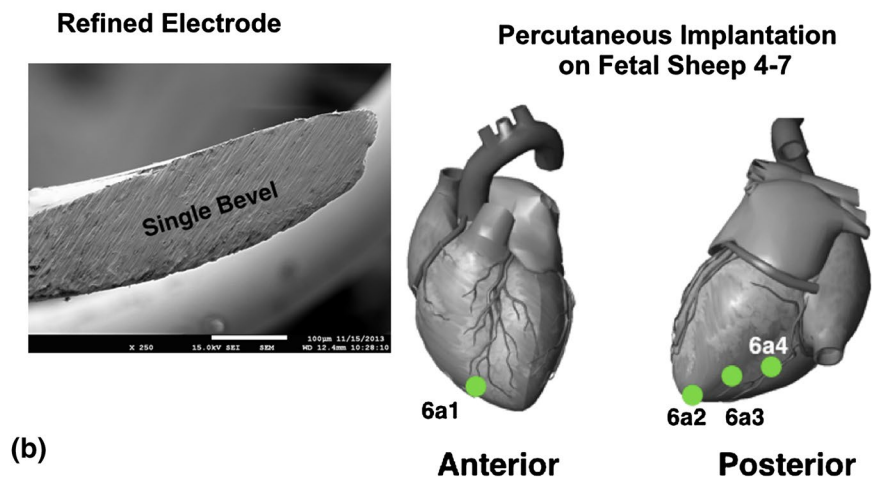
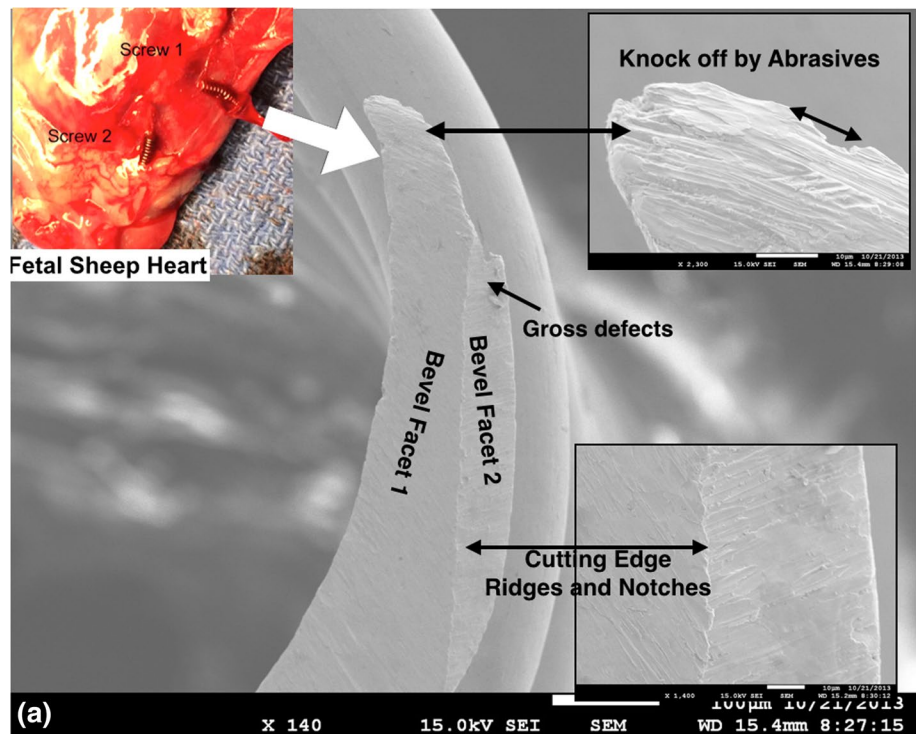


Fig. 4 Map of the in vivo electrode implantation attempts: sites 1a–1m were implanted with iridium corkscrew electrodes on surgically exposed rabbits’ hearts (wire diameter 150 μm , coil 1.3 mm diameter by 4.0 mm long, pitch 0.5 mm). Sites 0a–0c were implanted with larger Ir electrode coils (2.2 mm diameter) before this design was abandoned due to mechanical instability. Sites 2a–2d represent unsuccessful attempts to implant the original Ir electrode design on fetal sheep model (see Fig. 5 for successful implantation sites of revised electrode)

epicardium, resulting in high insertion force and incomplete penetration, high capture threshold, deformation of the electrode coil, unintended device release or abandonment of the implantation.

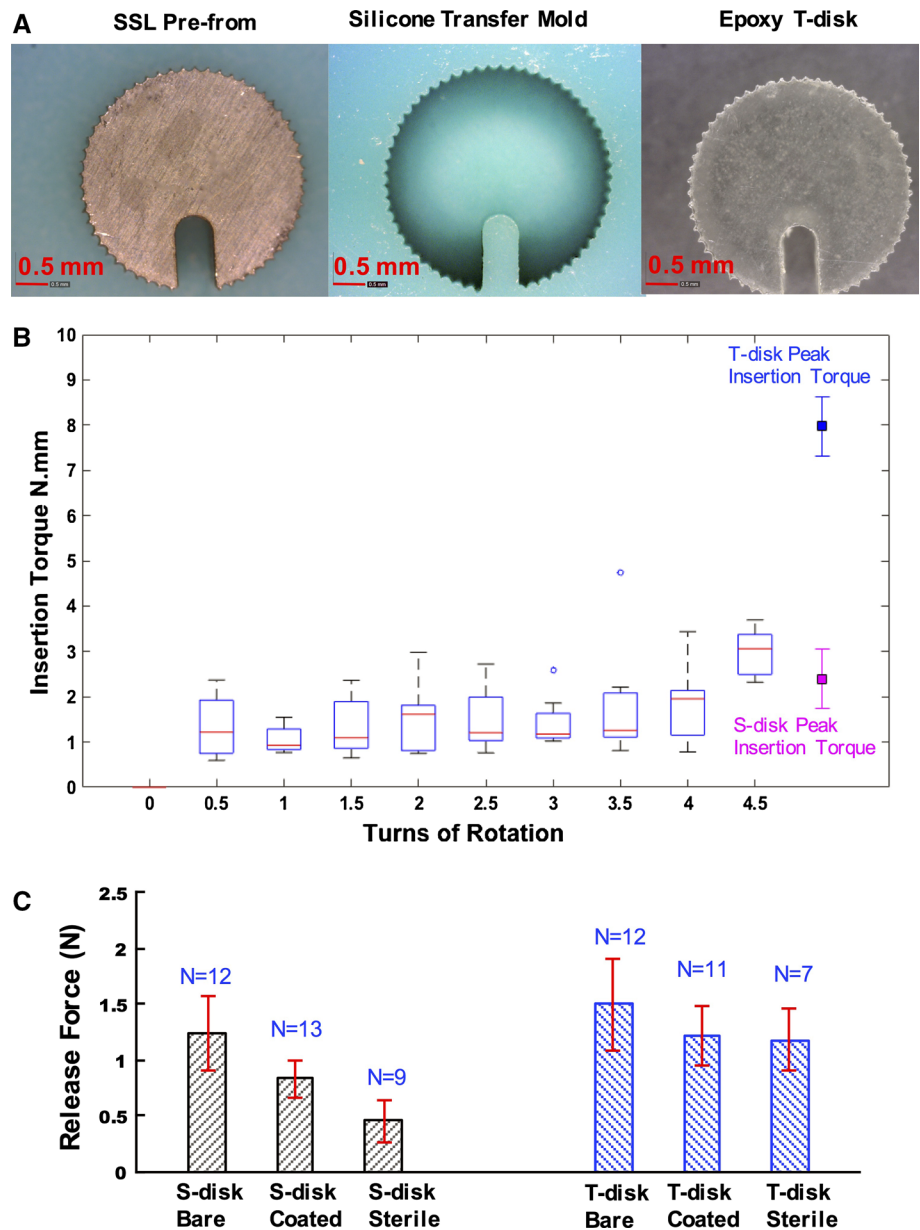
Fig. 5 Examination of the electrode tips under scanning electron microscope. **a** Micrograph of the iridium corkscrew electrode that was unable to be inserted in the RV of fetal sheep 2. **b** Revised electrode with single bevel facet and the sites of successful, ultrasonically guided implantations in sheep 4–7



Optimal Shape of Electrode Tip Okamura et al. [33] characterized the effects of needle diameter and tip shape on the cutting forces of needle insertion into soft tissue. Their result suggests the triangular tips (two intersected bevels) have the lowest frictional force, single bevel tips have intermediate force and cone tips have the highest force into soft tissue. This is a logical progression because the number of sharp edges corresponds to the ease of crack propagation and therefore cutting forces. Therefore, we compared electrode tips with a single bevel to those with a double-beveled triangular shape when implanted into a pig cadaver heart high on the RV free wall region, which was the most difficult location for implantation.

Surprisingly, the double-beveled tips actually exhibited higher insertion resistance than the single-beveled tips. Electrodes were examined under the scanning electron microscope. The micrograph in Fig. 5 indicates that the triangular tip forms a rough cutting edge at the intersection of the two beveled planes. Presumably, the ridges and notches left by the abrasive particles snag more collagen fibers. On the contrary, the single-beveled tips have less rough edges that cut rather than trap the connective tissue to produce less resistance during insertion. We further refined the sharpening technique by changing the grinding abrasive from 180 grit (abrasive particle size: 82 µm) to a finer 240 grit (53 µm).

Fig. 6 Insertion torque and release force. **a** The transfer molding process to fabricate the toothed friction disk (T-disk). The laser-cut stainless steel (SSL) preform has a thickness of 1.5 mm (same with original design). **b** The torque (median with 25–75 % box and full range in dashed lines) required to advance the Ir electrodes according to number of turns into pig myocardium (4 LV + 5 RV) compared to maximal torque (mean ± SD, $N = 20$) at which slip occurred between the plastic sheath and the S-disks vs. T-disks (Parylene-coated and EtO sterilized after lodging in sheath). **c** The axial release force (mean with 95 % confidence interval) for S-disks and T-disks at different stages of fabrication: Bare = epoxy as molded, Coated = Parylene-C, Sterile = exposed to EtO after lodging in sheath



Enhancement on Mechanical Stability Buckling deflection of the helical corkscrews (ϕ wire = 150 μm) was also observed when the corkscrew was turned into the connective tissue layer on the RV. For a helical spring with freely moving ends under combined compression and torsion [18], stability can be estimated from:

$$\frac{W}{\chi} \approx \frac{Kd^4}{2\pi Dn_0}$$

$$\frac{P}{\xi} \approx C\alpha_0 \left(\frac{d^2}{D}\right)^2$$

where W is the torque; χ is the degree of twisting; K and C are the material constant; d is the wire diameter; D is the coil diameter; n_0 is the number of the turns; α_0 is related to the pitch; ξ is the elongation; P is pressure; W/χ is the lateral stability against torque; and P/ξ is the stability against compression.

The wire diameter d has a substantial effect on the spring stability. We changed the iridium wire diameter from 150 to 254 μm , which should improve the lateral rigidity and the elastic stability by 7.7 times (keeping other parameters constant). The adjustment of the pitch from 0.5 to 1 mm changes n_0 from 8 to 4 turns for the same length corkscrew (4–4.5 mm in accordance

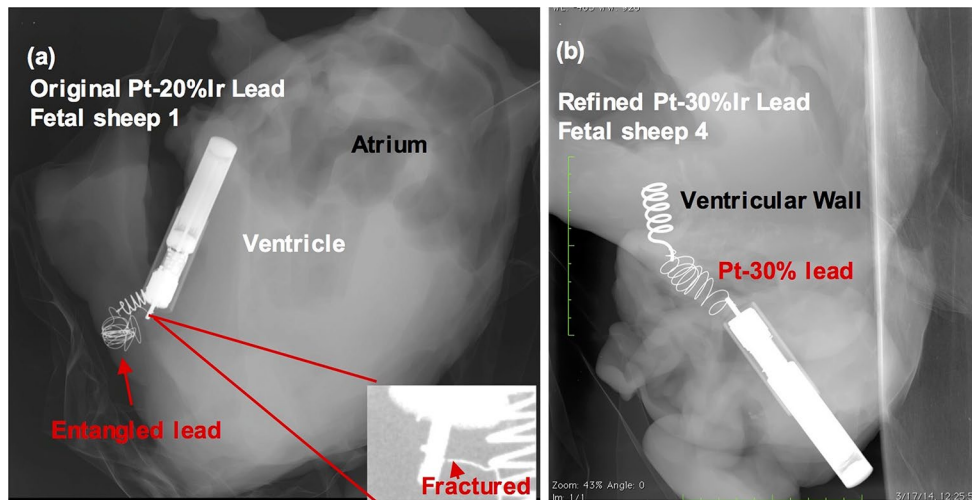


Fig. 7 High-resolution X-ray evaluation of the flexible lead performance in fetal sheep studies. **a** The original lead made from the annealed Pt-20%Ir was severely deformed. The image was obtained

1 month after implantation. **b** The refined new lead with Pt-30%Ir performed significantly better. The image was acquired 15 days after implantation

with 80 % of predicted ventricular wall thickness for a human fetus at 27–34 gestational weeks [24]. This does not affect the elastic stability, but it improves the lateral rigidity by 15.4 times when combined with the increase in wire diameter. The coil diameter was adjusted from 1.3 to 1.5 mm to compensate for the difficulty of winding the thicker iridium wire in a tight radius. These modifications significantly improved the mechanical stability. After the systematic refinement, the implantation was successful on both the RV and LV in subsequent *in vivo* fetal sheep experiments 4–7 shown in Fig. 7b. The thicker Ir wire might be expected to produce slightly more myocardial tissue displacement during implantation, but it might also distribute any residual forces on the tissue over a larger surface area, reducing local compression that could cut off capillary blood flow.

Ability to Apply Torque to the Electrode Figure 6 provides a comparison of the torques and forces required to insert and release Ir electrodes (with improved sharpening) to the maximal torques and forces that could be applied via the plastic sheath to the toothed T-disk (Fig. 6a) compared to the smooth S-disk (Fig. 1c friction disk). As shown in Fig. 6b, the torque rises when the disk bottoms on the epicardial surface. The original S-disk had a very low safety margin over the torque and insertion force (Fig. 6c) after sterilization compared to the T-disk. The softening of the polyimide sheath during EtO sterilization tends to loosen the friction grip on the S-disk but actually facilitates penetration of the T-disk teeth into the sheath wall, improving the grip.

3.2 Lead performance

In the first fetal sheep implantation, the flexible lead broke at a location close to the welding joint to the platinum rod of the pulse generator. The high-resolution X-ray image (Fig. 7a) also demonstrated that the flexible lead was too ductile to maintain the mechanical form of a helical coil. It plastically deformed into furling loops, which would no longer distribute the bending moments along the lead evenly, resulting in a stress riser where the lead was attached to the electronics package. In addition, the Parlylene-C insulation at the weld site was removed by heating with a hot filament pen (temperature above 1000 °C), which probably further annealed the PtIr alloy, increasing its ductility near this stress riser. In subsequent experiments, the polymer sleeve was carefully scraped off using a scalpel to avoid annealing. The alloy was switched to Pt-30%Ir alloy as-drawn instead of the original Pt-20%Ir annealed wire, providing both higher tensile strength and lower ductility [30]. In the postmortem analysis of sheep 4–7 (four pacing leads tested), the Pt-30%Ir lead maintained its helical structure (Fig. 7b) and no fractures were observed up to the longest *in vivo* observation of 15 days.

4 Discussion

4.1 Mechanical analysis of epicardial electrode insertion

Mechanical Aspect Mechanical properties of epicardium are dramatically different from those of

endocardium [22]. Epi-myocardium is designed to sustain significant in-plane biaxial loads [20]. For minimally invasive epicardial access, the design of the corkscrew electrode must consider the full range of insertion resistance that might be encountered on the outer surface of a heart. The electrode must be stiff and sharp enough so as to make the insertion process easy.

Ventricular Wall Architecture LeGrice et al. [25] describe ventricular myocardium as consisting of a three-dimensional organization of discrete laminar muscle layers and loosely coupled branching myocytes and perimysial collagen fiber meshwork connecting adjacent layers. Transmural variations exist regarding myocyte arrangement, perimysial fiber lengths, and numbers of branches between adjacent layers (branching density) from the outer to inner wall. The RV has a compliant structure that by nature can absorb more mechanical stresses.

The epicardium is the outer layer of the heart. It is a single layer of epicardial membrane connected to the myocardium by a layer of subepicardial adipose tissue (fat) [28]. The epicardial membrane is comprised of aligned collagen fibers and an interfibrillar elastin matrix plus small amounts of other fillers [37]. The collagen fibers are oriented in three principal directions at solid angles of $\pm 120^\circ$ [10]. It is noteworthy that the epicardial membranes of the right and left ventricles exhibit quantitatively similar biomechanical behaviors according to biaxial stress–strain experiments on excised canine ventricular epicardium. The stress–strain behavior of epicardial membrane is highly nonlinear, being initially compliant at low stretch ratio (16 % equibiaxial stretch in x and y directions; ~40 % uniaxial stretch in x or y direction) but then very stiff near the limits of extensibility (26 % equibiaxial, 60 % uniaxial) [20].

Strain Energy-based Model to Analyze the Cutting Process of Epicardial Membrane The ability of the corkscrew electrode to penetrate the epicardium depends on how easily the sharpened electrode tip can cut through the connective tissue membrane. Once the electrode is inserted against the connective tissue matrix, the membrane is elastically deformed by the realignment of interfibrillar elastin networks. As the strain continues, the bundled collagen fibers will be redistributed and aligned to produce a significant tensile resistance before fracture. Therefore, the external work (cutting force \times distance) is temporarily stored in the strained membrane and will be fully released when the fibers are cut. The Eq. 1 describes the cutting and fracture mechanisms of the thin biological membrane proposed by Doran et al. [9]:

$$Xu = d\Lambda + Jd\Gamma - dU \quad (1)$$

where Xu is the external work applied by rotation (X force; u displacement). $d\Lambda$ is elastic energy due to the deformation of the collagen network, which is a function of u . J is the fracture toughness of the epicardial membrane. $Jd\Lambda$ is the work absorbed by the membrane creating the new crack surface. $d\Lambda$ is the area of the crack surface area, which is determined by the cross-sectional area of the coil and its bevels. $d\Gamma$ is the energy lost in remote plastic flow, which may be substantial from slippage of the subepicardial adipose tissue. The term dU is the internal strain energy in the membrane from resting tension.

This analysis implies that the LV is easier to penetrate than the RV (requiring less Xu), because the membrane on the LV is under tension before cutting (high dU) and $d\Gamma$ is negligible because the LV has a sparse amount of subepicardial fat (assuming same $d\Lambda$ and $Jd\Lambda$ generated by the rotation of the same electrode on each ventricle).

Importantly, the design of the electrode tip plays a significant role in membrane cutting. First, it affects the numbers of collagen fibers snagged during the cutting. Reduction in the snagged collagen fibers can substantially minimize the energy absorbed by the elastic deformation in the collagen fiber network $d\Lambda$. Secondly, the tip shape can directly change the initial crack surface area under sharp edges so it affects the term ($d\Lambda$). A sufficiently sharp cutting surface can minimize remote plastic flow $d\Gamma$.

4.2 Limitations

The development of the fetal micropacemaker has been a constant iteration process, which inevitably requires design and testing. The preclinical trial in fetal sheep model is not an exact model of the human hydroptic fetus. The lack of pericardial effusion in the healthy experimental fetal model results in technical difficulty in inserting the cannula into the pericardial space in order to directly engage the electrode tip into the myocardium. This was addressed in our experiments by the injection of saline in the pericardial space prior to cannula insertion in order to create an iatrogenic pericardial effusion. However, this model still does not replicate a hydroptic fetus.

5 Conclusion

We have identified and addressed the potential mechanical failures and design risks of the fetal micropacemaker system. We identified and overcame the challenges of electrode fixation on the right ventricle via the percutaneous implantation approach. The fixation system was optimized after a thorough mechanical analysis of the insertion

process. By selecting the proper material and refining the fabrication techniques, the flexible lead successfully maintained its mechanical integrity after being implanted in fetal sheep. Further research will be needed to demonstrate whether the fetal micropacemaker is a viable option for treatment of this generally fatal condition.

Acknowledgments This research was funded by an NIH R01 Grant (1R01HD075135), the Southern California Clinical and Translational Science Institute, Robert E. and May R. Wright Foundation, and the Coulter Foundation. Some aspects of the mechanical design and fabrication are the subject of pending patent applications by Children's Hospital of Los Angeles. No commercial partnerships have yet been arranged.

References

- Abrams ME, Meredith KS, Kinnard P, Clark RH (2007) Hydrops fetalis: a retrospective review of cases reported to a large national database and identification of risk factors associated with death. *Pediatrics* 120:84–89
- Assad RS, Zielinsky P, Kalil R, Lima G, Aramayo A, Santos A, Costa R, Marcial MB, Oliveira SA (2003) New lead for in utero pacing for fetal congenital heart block. *J Thorac Cardiovasc Surg* 126:300–302
- Ball R, Golombeck K, Jacobs V, Lee H, Farrell J, Farmer D, Filly R, Rosen M, Harrison M (2004) Maternal morbidity after fetal surgery. *Am J Obstet Gynecol* 191:S10
- Bar-Cohen Y, Loeb GE, Pruetz JD, Silka MJ, Guerra C, Vest AN, Zhou L, Chmait RH (2015) Preclinical testing and optimization of a novel fetal micropacemaker. *Heart Rhythm* 12(7):1683–1690
- Breur JM, Kapusta L, Stoutenbeek P, Visser GH, Van Den Berg P, Meijboom E-J (2008) Isolated congenital atrioventricular block diagnosed in utero: natural history and outcome. *J Matern Fetal Neonat Med* 21:469–476
- Carpenter RJ Jr, Strasburger JF, Garson A Jr, Smith RT, Deter RL (1986) Fetal ventricular pacing for hydrops secondary to complete atrioventricular block. *J Am Coll Cardiol* 8:1434–1436
- Chatelain P, Adamec R, Cox J (1985) Morphological changes in human myocardium during permanent pacing. *Virchows Archiv A* 407:43–57
- Danzer E, Sydorak RM, Harrison MR, Albanese CT (2003) Minimal access fetal surgery. *Eur J Obstet Gynecol Reprod Biol* 108:3–13
- Doran C, McCormack B, Macey A (2004) A simplified model to determine the contribution of strain energy in the failure process of thin biological membranes during cutting. *Strain* 40:173–179
- Dunn MG, Silver FH (1983) Viscoelastic behavior of human connective tissues: relative contribution of viscous and elastic components. *Connect Tissue Res* 12:59–70
- Eghtesady P, Michelfelder EC, Knilans TK, Witte DP, Manning PB, Crombleholme TM (2011) Fetal surgical management of congenital heart block in a hydroptic fetus: lessons learned from a clinical experience. *J Thorac Cardiovasc Surg* 141(3):835–837
- Eliasson H, Sonesson S-E, Sharland G, Granath F, Simpson JM, Carvalho JS, Jicinska H, Tomek V, Dangel J, Zielinsky P (2011) Isolated atrioventricular block in the fetus: a retrospective, multinational, multicenter study of 175 patients. *Circulation* 124:1919–1926
- Escobar-Diaz MC, Tworetzky W, Friedman K, Lafranchi T, Fynn-Thompson F, Alexander ME, Mah DY (2014) Perinatal outcome in fetuses with heterotaxy syndrome and atrioventricular block or bradycardia. *Pediatr Cardiol* 35(6):906–913
- Fesslova V, Vignati G, Brucato A, De Sanctis M, Butera G, Pia Pisoni M, Chiappa E, Acaia B, Meroni PL (2009) The impact of treatment of the fetus by maternal therapy on the fetal and postnatal outcomes for fetuses diagnosed with isolated complete atrioventricular block. *Cardiol Young* 19:282–290
- Friedman DM, Llanos C, Izmirly PM, Brock B, Byron J, Copel J, Cummskey K, Dooley MA, Foley J, Graves C (2010) Evaluation of fetuses in a study of intravenous immunoglobulin as preventive therapy for congenital heart block: results of a multicenter, prospective, open-label clinical trial. *Arthritis Rheum* 62:1138–1146
- Grethel EJ, Wagner AJ, Clifton MS, Cortes RA, Farmer DL, Harrison MR, Nobuhara KK, Lee H (2007) Fetal intervention for mass lesions and hydrops improves outcome: a 15-year experience. *J Pediatr Surg* 42:117–123
- Groves AM, Allan LD, Rosenthal E (1995) Therapeutic trial of sympathomimetics in three cases of complete heart block in the fetus. *Circulation* 92:3394–3396
- Haringx J (1947) On highly compressible helical spring and rubber bars and their application in vibration isolation. Doctoral Thesis, Delft University of Technology, The Netherlands
- Ho SY, Esscher E, Anderson RH, Michaëlsen M (1986) Anatomy of congenital complete heart block and relation to maternal anti-Ro antibodies. *Am J Cardiol* 58:291–294
- Humphrey J, Strumpf R, Yin F (1990) Biaxial mechanical behavior of excised ventricular epicardium. *Am J Physiol Heart Circ Physiol* 259:H101–H108
- Jaeggi ET, Hamilton RM, Silverman ED, Zamora SA, Hornberger LK (2002) Outcome of children with fetal, neonatal or childhood diagnosis of isolated congenital atrioventricular block: a single institution's experience of 30 years. *J Am Coll Cardiol* 39:130–137
- Kang T, Humphrey J, Yin F (1996) Comparison of biaxial mechanical properties of excised endocardium and epicardium. *Am J Physiol Heart Circ Physiol* 270:H2169–H2176
- Kohl T, Strümper D, Witteler R, Merschhoff G, Alexiene R, Caltenbeck C, Asfour B, Reckers J, Aryee S, Vahlhaus C (2000) Fetoscopic direct fetal cardiac access in sheep an important experimental milestone along the route to human fetal cardiac intervention. *Circulation* 102:1602–1604
- Kurtoglu Z, Uluutku M, Yeginoglu G, Ozturk H, Camdeviren H (2004) Ventricular myocardial thicknesses in anencephalic fetuses. *Clin Anat* 17:492–496
- LeGrice IJ, Smaill B, Chai L, Edgar S, Gavin J, Hunter PJ (1995) Laminar structure of the heart: ventricular myocyte arrangement and connective tissue architecture in the dog. *Am J Physiol Heart Circ Physiol* 269:H571–H582
- Loeb GE, Zhou L, Zheng K, Nicholson A, Peck RA, Krishnan A, Silka M, Pruetz J, Chmait R, Bar-Cohen Y (2013) Design and testing of a percutaneously implantable fetal pacemaker. *Ann Biomed Eng* 41:17–27
- Lopes LM, Tavares GMP, Damiano AP, Lopes MAB, Aiello VD, Schultz R, Zugaib M (2008) Perinatal outcome of fetal atrioventricular block one-hundred-sixteen cases from a single institution. *Circulation* 118:1268–1275
- Männer J, Perez-Pomares J, Macias D, Munoz-Chapuli R (2000) The origin, formation and developmental significance of the epicardium: a review. *Cells Tissues Organs* 169:89–103
- McElhinney DB, Tworetzky W, Lock JE (2010) Current status of fetal cardiac intervention. *Circulation* 121:1256–1263
- Merker J, Lupton D, Töpfer M, Knake H (2001) High temperature mechanical properties of the platinum group metals. *Platin Met Rev* 45:74–82

31. Merrill DR, Bikson M, Jefferys JG (2005) Electrical stimulation of excitable tissue: design of efficacious and safe protocols. *J Neurosci Methods* 141:171–198
32. Michaelsson M, Engle MA (1972) Congenital complete heart block: an international study of the natural history. *Cardiovasc Clin* 4:85
33. Okamura AM, Simone C, O’Leary MD (2004) Force modeling for needle insertion into soft tissue. *Biomed Eng IEEE Trans* 51:1707–1716
34. Pisoni C, Brucato A, Ruffatti A, Espinosa G, Cervera R, Belmonte-Serrano M, Sánchez-Román J, García-Hernández F, Tincani A, Bertero M (2010) Failure of intravenous immunoglobulin to prevent congenital heart block: findings of a multicenter, prospective, observational study. *Arthritis Rheum* 62:1147–1152
35. Robblee L, Lefko J, Brummer S (1983) Activated Ir: an electrode suitable for reversible charge injection in saline solution. *J Electrochem Soc* 130:731–733
36. Schmidt KG, Ulmer HE, Silverman NH, Kleinman CS, Copel JA (1991) Perinatal outcome of fetal complete atrioventricular block: a multicenter experience. *J Am Coll Cardiol* 17:1360–1366
37. Silver F, Kato Y, Ohno M, Wasserman A (1991) Analysis of mammalian connective tissue: relationship between hierarchical structures and mechanical properties. *J Long Term Eff Med Implant* 2:165–198
38. Strasburger JF, Wakai RT (2010) Fetal cardiac arrhythmia detection and in utero therapy. *Nat Rev Cardiol* 7:277–290
39. Taylor PV, Scott JS, Gerlis LM, Esscher E, Scott O (1986) Maternal antibodies against fetal cardiac antigens in congenital complete heart block. *N Engl J Med* 315:667–672
40. Walkinshaw S, Welch C, McCormack J, Walsh K (1994) In utero pacing for fetal congenital heart block. *Fetal Diagn Ther* 9:183–185



Raymond A. Peck is a Mechanical Engineer specializing in the electromechanical design and fabrication of implantable medical devices, including implantable micropumps, RF neuromuscular stimulators, and cochlear electrode arrays.



Jonathan P. Sredl completed his Master of Science degree in Biomedical Engineering with a specialization in Neuroengineering. He is currently working in healthcare policy and analytics in Bethesda, MD.



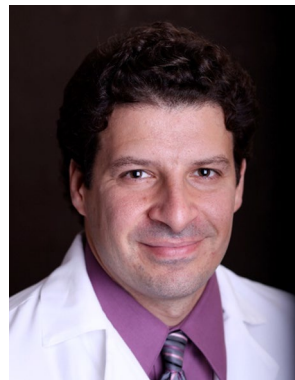
Li Zhou completed his master degree in materials science and his Ph.D. in Biomedical Engineering with a focus on medical device design and development at University of Southern California.



Xuechen Huang is currently a Provost Fellow working toward his Ph.D. degree in applied neurophysiology in Biomedical Engineering Department at University of Southern California, Los Angeles.



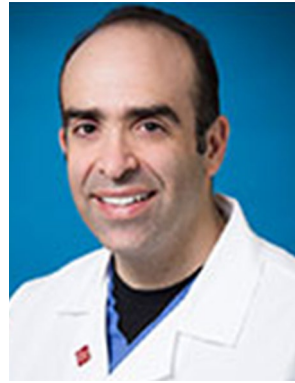
Adriana Nicholson Vest completed her Ph.D. in Biomedical Engineering with a focus on electrophysiology and instrumentation. She is currently a postdoctoral fellow at Georgia Institute of Technology.



Yaniv Bar-Cohen, MD, is a pediatric electrophysiologist and the Director of Cardiac Rhythm Devices at CHLA. He is an Associate Professor of Pediatrics and Medicine at the Keck School of Medicine at the University of Southern California.



Michael J. Silka, MD, is a Professor of Pediatrics/Cardiology and Director of Cardiac Electrophysiology, Children's Hospital Los Angeles, University of Southern California. He is a past president of the Pediatric Electrophysiology Society.



Ramen H. Chmait, MD, is an Associate Professor of Obstetrics and Gynecology at the University of Southern California, Keck School of Medicine, and Director of Los Angeles Fetal Surgery.



Dr. Jay D. Pruetz is an Assistant Professor of Pediatrics at the University of Southern California (USC) and director of the fetal cardiology program in the division of pediatric cardiology at Children's Hospital Los Angeles (CHLA).



Gerald E. Loeb, MD, Johns Hopkins, NIH (1973–1988), Prof. Physiology, Queen's Univ. (1988–1999); now Prof. Biomedical Engineering and Dir. Medical Device Development Facility, Univ. Southern California.